

Electronic Supplementary Information for: Thermodynamic Insights into the Self-assembly of Zeolitic Imidazolate Frameworks from Computer Simulations

Emilio Méndez and Rocio Semino*

*Sorbonne Université, CNRS, Physico-chimie des Electrolytes et Nanosystèmes Interfaciaux,
PHENIX, F-75005 Paris, France.*

E-mail: rocio.semino@sorbonne-universite.fr

Index

Well-tempered metadynamics setup, 2

Convergence and uncertainty calculation, 3

Transformations of the collective variable space, 5

ZIF surface generation, 6

Pentacoordinated intermediate species for the addition of a third ligand to (010) and (001)

ZIF-4 surfaces, 8

Force field parameters, 8

Force field validation: structure, 11

Force field validation: electronic structure calculations, 14

Well-tempered metadynamics setup

The parameters for the well-tempered metadynamics simulations were set as follows:

- the initial gaussian height was set equal to kT ,
- the pace was set equal to 1000 (a new Gaussian is deposited every 1000 timesteps),
- the gaussian widths were 0.1 for the coordination number collective variables (CVs) and 0.5 Å for the distance CVs, and
- the bias factor that controls the decay of the heights with time was chosen to be 30.

Five parallel walkers were employed to accelerate the convergence.¹ Each walker evolves independently from the others but they all share the same bias potential obtained from the addition of gaussian terms. The total time for each simulation, comprising all the walkers, was around 150 ns.

In the case of the simulations that involve a crystal slab, the coordination number between the reactive Zn^{2+} /ligand and all the free surface N/Zn other than the ones that belong to the tagged site was kept fixed and equal to zero. Upper and lower boundaries were imposed to the CVs to avoid the exploration of non-physical regions and to keep the Zn^{2+} within a distance lower than 10 Å from the surface, at which the free energy already reaches a plateau.

For the formation of early complexes, we employed cubic simulation boxes containing 112 solvent molecules plus the reactive ions (one Zn and two imidazolate ligands -step 1- and two Zn and four imidazolate ligands -step 2). The average volume was around 15.6 nm³. For the addition of ions to a pre-formed slab, the systems were composed as follows: ZIF-4 (100): 97 Zn and 362 DMF. ZIF-4 (010): 137 Zn and 363 DMF. ZIF-4 (001): 121 Zn and 311 DMF. ZIF-1 (010): 100 Zn and 222 DMF. The amount of ligands was twice the amount of Zn in all cases. The average box dimensions were approximately twice the ZIF lattice parameters

in the directions perpendicular to the growth and four times the lattice parameter in the growing direction (see "ZIF surface generation Section").

Convergence and uncertainty calculation

To analyze the convergence of the well-tempered metadynamics simulations we followed the procedure developed by Tiwary *et al.*² This approach takes into account the fact that the bias potential is dynamically modified as the metadynamics simulation advances and it never reaches a plateau value. This makes it non trivial to choose a convergence criterion. Tiwary and coworkers found a way to compute a time independent free energy estimator that allows to compare results measured at different times during the simulation given by:

$$G(s) = -\frac{\gamma V(s, t)}{(\gamma - 1)} + k_b T \ln \int e^{\frac{\gamma V(s, t)}{(\gamma - 1) k_b T}} ds \quad (1)$$

where s represents the collective variable(s), γ the bias factor, and $V(s, t)$ the time dependent bias potential. The last term of Eq. 1 is a time dependent constant that aligns the free energy estimation at time t with the ones computed at previous times. In order to apply this technique to data obtained from different walkers, we ordered the gaussians coming from each simulation as a function of time. As an example, in Fig. 1 we plotted the free energy estimator of Eq. 1 as a function of time for three points in the CV space for the reaction that involves the bonding of two imidazolate ions to a Zn ion. The points correspond to (i) $d_1=2 \text{ \AA}$, $d_2=6 \text{ \AA}$, $n_{Zn-O}=4$ (ii) $d_1=6 \text{ \AA}$, $d_2=2 \text{ \AA}$, $n_{Zn-O}=4$ and (iii) $d_1=6 \text{ \AA}$, $d_2=6 \text{ \AA}$, $n_{Zn-O}=6$, where d_1 and d_2 are the distances between the Zn and the tagged imidazolate moieties and n_{Zn-O} is the number of solvent molecules surrounding the Zn ion. The first two points are equivalent and correspond to a situation where one of the imidazolate ions is bonded to the Zn and other one is not. The fact that both curves lie close to each other is another indicator of the convergence of the simulation. The third point is higher in energy and corresponds to a situation where both ligands are dissociated from the Zn ion. We also

plotted the free energy without the addition of the second term of Eq. 1. As expected, these last values continue to descend without reaching a plateau, but the corrected estimators fluctuate around constant values.

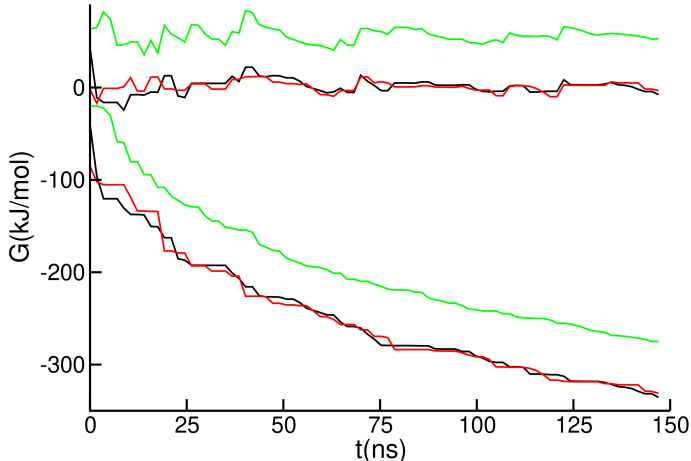


Figure 1: Free energy estimator for three representative points in the CV space for the reaction that involves the bonding of two imidazoles to a Zn ion. The curves in the negative region correspond to the estimator without the second term of Eq. 1. The black, red and green curves correspond to the three points described in the text, respectively.

In order to compute the final free energy profile and the corresponding errors, we need to time average the results from the corrected free energy curves. To avoid artifacts that arise when dealing with correlated data, we employed the block averaging technique developed by Bussi and Tribello.³ To estimate the optimal block size for which the data is uncorrelated, we computed the standard deviation of the free energy as a function of the block size. Results associated to the lowest energy structure are shown in figure 2. When the individual block values become uncorrelated, the standard deviation reaches a plateau. According to this criterion, we averaged data from blocks of 13 ns. This procedure was performed for all the reactions studied.

Transformations of the collective variable space

It was often necessary to perform some kind of coordinate transformation or dimensionality reduction to have a clearer visualization of the free energy curves. All the modifications

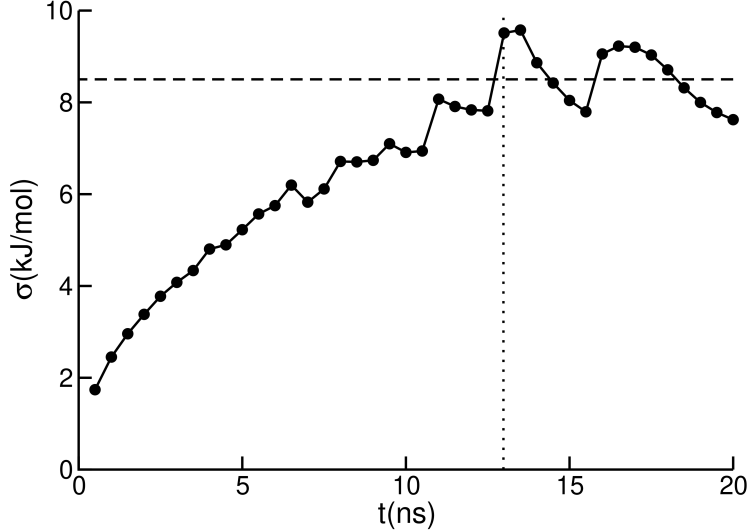


Figure 2: Standard deviation of the free energy associated to the absolute minimum as a function of the block size, for the same reaction as in Fig. 1. The vertical line indicates the value at which we consider the results to be uncorrelated. The horizontal line indicates the average standard deviation after the decorrelation time is reached.

applied rely on the relationship between the free energy G as a function of the CVs (ξ_1 , ξ_2 and ξ_3) and the probability distribution function $\mathcal{P}(\xi_1, \xi_2, \xi_3)$:

$$\mathcal{P}(\xi_1, \xi_2, \xi_3) = C e^{-\beta G(\xi_1, \xi_2, \xi_3)} \quad (2)$$

where C is a normalization constant. The undesired CVs can be integrated from the probability distribution function in order to reduce the dimensionality of the free energy surface. Then, the free energy in the reduced space is obtained by inverting Eq. 2.

In the first section of the results we applied the following transformation for computing G as a function of the Zn-Im coordination number (n_{Zn-N}^*) from $G(d_1, d_2)$. We computed the probability of the new variable by:

$$\mathcal{P}(n_{Zn-N}^*) = \int \delta(n_{Zn-N}^* - n_{Zn-N}(d_1, d_2)) \mathcal{P}(d_1, d_2) dd_1 dd_2 \quad (3)$$

where the function $n_{Zn-N}(d_1, d_2)$ follows the definition given in the main text. In practice, this integration is performed numerically by discretizing the CV space into finite bins. Sub-

sequently, the free energy was recovered by the inversion of Eq. 2. The uncertainties of the transformed free energies were computed from the ones that correspond to the original curves by propagation of errors.

ZIF surface generation

In order to create the crystal-solvent interfaces described in section 'ZIF crystal growth' of the article we proceeded as follows:

- (i) Starting from a ZIF-4 unit cell we filled the system with solvent using a grand canonical Monte Carlo (GCMC) procedure until the experimental loading of 8 DMF molecules was reached.⁴
- (ii) The system was then replicated twice in each direction parallel to the desired surface and four times in the direction perpendicular to it. For example, to construct a surface slab with a normal in the z direction, we should multiply the original unit cell by $2 \times 2 \times 4$.
- (iii) In order to cut the system and generate the interface, we deleted all the atoms that lied outside the central $2 \times 2 \times 2$ region. Imidazolate moieties that were half-cut during this procedure were completely removed.
- (iv) We randomly deleted some of the surface Zn, taking care that both surfaces have the same amount of exposed Zn and ligands and that the charge neutrality was maintained. This was done so that the net dipole of the final structure in the direction perpendicular to the surface was zero.
- (v) The empty space generated after cutting the MOF, which occupies half of the simulation box, was filled with solvent via GCMC simulations as done before. The central surface slab was kept frozen during this step.

- (vi) To avoid any further degradation in the surface other than the desired reaction, we forced the Zn-imidazolate connectivity to remain unaltered in all cases except for that of the tagged Zn ion or ligand that will be adsorbed/desorbed into the surface. This was done by adding extra harmonic bonds between neighbor Zn and N atoms. These constraints do not produce any significant structural change in the crystalline slab.
- (vii) A short preliminary run of ~ 1 ns was performed to allow the system to equilibrate.

This scheme was also applied for the generation of the ZIF-1 slab. In this case, given the lack of experimental information about the solvent filled structure, we added 24 DMF molecules per unit cell. This corresponds to one molecule per pore in the system, which is equivalent to what was found for ZIF-4, and seems to represent the most stable configuration obtained via GCMC.

Pentacoordinated intermediate species for the addition of a third ligand to (010) and (001) ZIF-4 surfaces

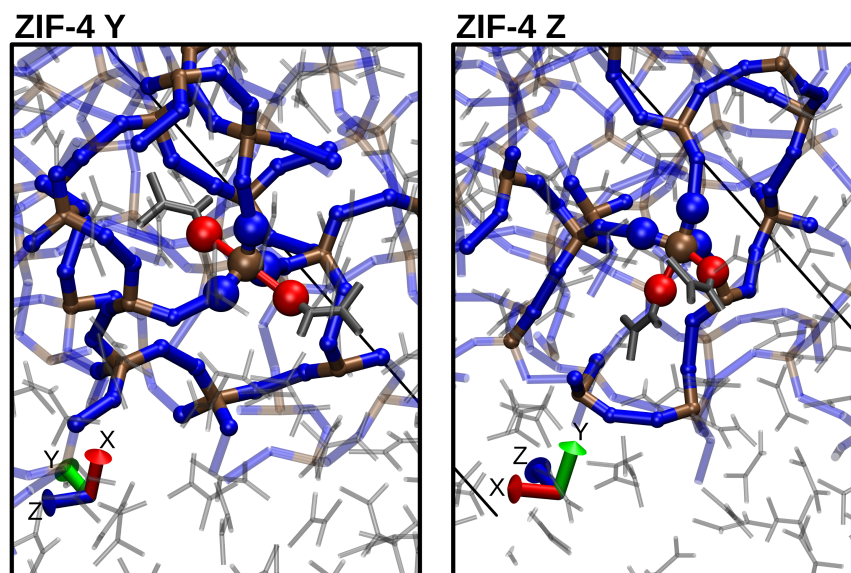


Figure 3: Typical snapshots of the intermediate species before the formation of the tri-coordinated Zn-imidazolate complex in the (010) and (001) ZIF-4 surface slabs (left and right respectively).

Force field parameters

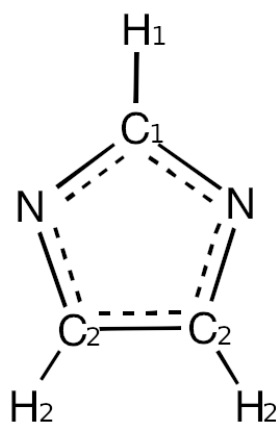


Figure 4: Representation of an imidazolate ion with the atom type name for each species.

The potential energy of the system E was described as a sum of the following contributions:

$$E = E_{coul-LJ} + E_{morse} + E_{bond} + E_{angle} + E_{dihedral} + E_{improper} \quad (4)$$

where $E_{coul-LJ}$ is the coulombic plus Lennard Jones energy and E_{morse} is the Morse energy, and together they constitute the non bonded interactions. E_{bond} , E_{angle} , $E_{dihedral}$ and $E_{improper}$ are the intramolecular contributions and refer to the bond, angular, dihedral and improper energies respectively. The formula employed for the calculation of $E_{coul-LJ}$ is the following:

$$E_{coul-LJ} = 4\epsilon \left[\left(\frac{\sigma}{r} \right)^{12} - \left(\frac{\sigma}{r} \right)^6 \right] + \frac{Cq_iq_j}{r} \quad (5)$$

where r is the interatomic distance, ϵ , σ and q are parameters that depend on the atomic species while C is a constant. ϵ and σ were obtained from single atom values by standard Lorentz-Berthelot mixing rules, with the exception of Zn-N(Im) and Zn-O(DMF) pairs that do not have Lennard Jones parameters since their interactions are modeled with Morse potentials. In figure 4 we indicate the name of each species in the imidazolate ion (Im). In table 1 we summarize the ϵ , σ and q values for all the present species. The species marked with a * symbol represent the dummy atoms, that are present in the Zn and N(Im) species. A six sites model was used for dimethylformamide (DMF), in which the methyl groups were considered as united atoms.⁵ Long range coulombic interactions were computed with the particle-particle particle-mesh method. The cutoff distance for other interactions was set to 13 Å. Non bonded interactions were not considered for first and second neighbor atoms, and were scaled by a factor of 0.5 (0.6874) for Lennard Jones (Coulombic) interactions. The Morse potential was computed using the following expression:

$$E_{morse} = D_0 \left[e^{-2\alpha(r-r_0)} - 2e^{-\alpha(r-r_0)} \right] \quad (6)$$

where D_0 , α and r_0 are parameters that are also displayed in table 1. Only Zn-N(Im)

and Zn–O(DMF) pairs contributed to the total energy with this kind of interaction.

The values of D_0 , α and r_0 for the Zn–N(Im) interaction were the only parameters that were changed with respect to the original nb-ZIF-FF. They were optimized simultaneously with the corresponding values from the Zn–O(DMF) interaction. This was done in such a way that the system reproduces two qualitative aspects observed experimentally: (i) the most stable Zn²⁺ complex in DMF should be octahedral⁶ and (ii) a ZIF-4 crystal filled with DMF should be stable at 400 K, which is the synthesis temperature.⁷

For the bonded terms the employed formulas are:

$$E_{bond} = K(r - r_0)^2 \tag{7}$$

$$E_{angle} = K(\theta - \theta_0)^2 + K_{ub}(r - r_{ub})^2 \tag{8}$$

$$E_{dihedral} = K[1 + \cos(n\phi - d)] \tag{9}$$

$$E_{improper} = K[1 + d\cos(n\phi)] \tag{10}$$

For these expressions, θ represents an angle, ϕ a dihedral or improper angle, and K , r_0 , θ_0 , K_{ub} , r_{ub} , n and d are parameters that are displayed in tables 2 and 3.

Table 1: Long range interaction parameters

Coulombic-Lennard Jones			
	q (e)	$\epsilon(10^{-3}\text{eV})$	$\sigma(\text{\AA})$
Zn	0.354	0.542	1.96
Zn*	0.088	0	-
N	0	7.376	3.25
N*	-0.42	0	-
C ₁	0.277	3.73	3.4
H ₁	0.114	0.681	2.47
C ₂	-0.066	3.731	3.4
H ₂	0.114	0.651	2.51
C _{DMF}	0.45	4.215	3.7
O _{DMF}	-0.5	9.467	2.96
N _{DMF}	-0.57	6.744	3.2
H _{DMF}	0.06	0.675	2.2
CH _{3DMF}	0.28	6.744	3.8
Morse			
	$D_0(\text{eV})$	$r_0(\text{\AA})$	$\alpha(\text{\AA}^{-1})$
Zn-N	0.2	2.0	4.0
Zn-O _(DMF)	0.5	2.1	4.0

Force field validation

We evaluated the performance of the adapted force field for modelling the crystalline phases as well as the solvated species. For the crystalline phases, we measured the deviations of some equilibrium properties of ZIF-4 with respect to both the original potential and the reference data. The energy difference between ZIF-1 and ZIF-4 is shown in table 4 for the adapted and original versions of nb-ZIF-FF together with data from *ab initio* calculations.⁸ In table 5 we show the cell parameters of ZIF-4 computed using both potentials and the experimental data.⁷ In table 6 we include interatomic distances and angles in ZIF-4. Finally we show the integral of the radial distribution function ($g(r)$) of Zn-N pairs in the right panel of Fig. 5. For the solvated species we measured the integral of the $g(r)$ of Zn-O(DMF) pairs in a system composed by a single Zn ion surrounded by DMF solvent molecules. Results are shown in the left panel of Fig. 5. From these results we can conclude that the force field is able to capture the geometrical changes in the Zn coordination shell that occur when passing from the solution (6-coordinated) to the crystalline phase (4-coordinated).

Table 2: Intramolecular interaction parameters (part 1). Species marked with * represent dummy atoms.

Bonds				
	$K(\text{eV}\text{\AA}^{-2})$		$r_0(\text{\AA})$	
Zn Zn*	23.41		0.9	
N C ₁	14.62		1.355	
N C ₂	12.55		1.386	
N N*	23.41		0.5	
C ₁ H ₁	16.03		1.088	
C ₂ H ₂	16.03		1.088	
C ₂ C ₂	17.44		1.377	
Zn* Zn*	23.41		1.47	
C H _{DMF}	13.74		1.123	
C O _{DMF}	28.19		1.23	
C N _{DMF}	18.65		1.33	
N CH _{3DMF}	10.41		1.44	
Angles				
	$K(\text{eV}^\circ\text{-}^2)$	$\theta_0(^\circ)$	$K_{ub}(\text{eV}\text{\AA}^{-2})$	$r_{ub}(\text{\AA})$
Zn* Zn Zn*	2.384	109.5	0	0
C ₁ N C ₂	2.008	106.25	4.841	2.193
C ₁ N N*	0.625	126.85	0	0
C ₂ N N*	0.492	126.95	0	0
N C ₁ N	1.402	111.17	4.655	2.236
N C ₁ H ₁	1.694	124.2	0.886	2.16
N C ₂ H ₂	1.369	121.32	0.886	2.16
N C ₂ C ₂	1.456	108	4.295	2.235
H ₂ C ₂ C ₂	130.03	130.03	0.641	2.236
Zn Zn* Zn*	2.384	35.5	0	0
Zn* Zn* Zn*	2.384	60	0	0
CH ₃ N CH _{3DMF}	2.17	121	0	0
CH ₃ N C _{DMF}	2.17	120	0	0
N C H _{DMF}	1.907	114.5	0	0
O C N _{DMF}	3.25	123	0	0
H C O _{DMF}	1.907	122.5	0	0

Table 3: Intramolecular interaction parameters (part 2)

Dihedrals			
	$K(\text{eV})$	n	$d(^{\circ})$
N C ₁ N C ₂	0.467	2	180
N C ₁ N N*	0.0266	2	180
N C ₂ C ₂ N	0.665	2	180
N C ₂ C ₂ H ₂	0.154	2	180
C ₁ N C ₂ H ₂	0.158	2	180
C ₁ N C ₂ C ₂	0.288	2	180
H ₁ C ₁ N C ₂	0.158	2	180
H ₁ C ₁ N N*	0.01	2	180
C ₂ C ₂ N N*	0.061	2	180
H ₂ C ₂ N N*	0.0458	2	180
H ₂ C ₂ C ₂ H ₂	0.015	2	180
H C N CH ₃ <i>DMF</i>	0.12	2	180
O C N CH ₃ <i>DMF</i>	0.12	2	180
Impropers			
	$K(\text{eV})$	d	n
N C ₁ C ₂ N*	0.152	-1	2
C ₁ N N H ₁	0.152	-1	2

Table 4: Energy difference between ZIF-4 and ZIF-1. The values are expressed in kJ/mol of Zn atoms.

	$\Delta E_{ZIF-4 \rightarrow ZIF-1}(\text{kJ/mol})$
nb-ZIF-FF(adapted)	1.73
nb-ZIF-FF(original)	1.13
Ab initio ⁹	1.59

Table 5: Cell parameters of ZIF-4 for both nb-ZIF-FF versions (original⁹ and current) and experimental data⁷.

	$a(\text{nm})$	$b(\text{nm})$	$c(\text{nm})$
nb-ZIF-FF(adapted)	1.49	1.53	1.73
nb-ZIF-FF(original)	1.49	1.52	1.77
Experimental	1.54	1.53	1.84

Table 6: Mean values of interatomic distances and angles in ZIF-4 for both nb-ZIF-FF versions (original⁹ and current) and *ab initio* data.^{10,11}

	$\langle d_{Zn-N} \rangle(\text{\AA})$	$\langle d_{Zn-Zn} \rangle(\text{\AA})$	$\langle \theta_{N-Zn-N} \rangle(^{\circ})$
nb-ZIF-FF(adapted)	1.9	5.7	109
nb-ZIF-FF(original)	1.9	5.8	109
Ab initio	2.0	5.9	109

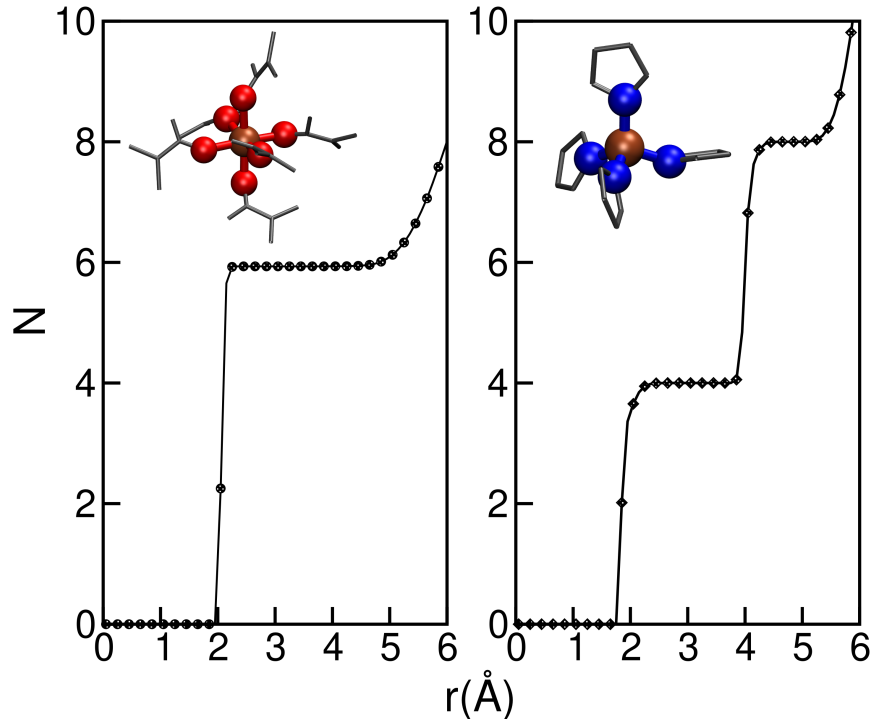


Figure 5: Integral of the radial distribution function of Zn-O pairs in a Zn solution in DMF (left) and Zn-N pairs in a ZIF-4 crystal (right).

Electronic structure calculations

To further evaluate the performance of the force field, we performed *ab initio* Density Functional Theory (DFT) optimization calculations to determine the energy of selected Zn-solvent, Zn-solvent-ligand and Zn-ligand clusters studied in the main text. The calculations were performed via the Quantum Espresso software,¹² which uses plane waves basis sets for modeling the electron density function. The atomic pseudo potentials were obtained from the Standard Solid State Pseudo Potentials database.¹³ High-precision pseudo potentials were used with PBE exchange correlation functional.¹⁴ Van del Waals corrections were included through the Grimme-D3 method.¹⁵ Implicit DMF solvent was modelled through the Environ package.¹⁶ The relative permittivity of DMF was set to 37.2.¹⁷ The Martyna-Tuckerman method was used to avoid interaction between periodic images.¹⁸ The atomic positions of all the structures were allowed to relax to the energy minimum before computing their energies.

The energy cutoff for the kinetic energy of the wave functions and the electron density were augmented until convergence was reached, giving a value of 80 and 320 Ry respectively. The same procedure was employed for obtaining the box size, resulting in 2 nm in each direction. Since the calculations involved isolated clusters, a single K-point was used to characterize the wave functions. For the geometry optimization, convergence thresholds of 10^{-4} Ry for the energy and 10^{-3} Ry/Bohr for the total forces were employed.

In table 7 we show the energy differences of five selected reactions computed with DFT and with nb-ZIF-FF. The first reaction involves the full conversion from the initial $[\text{Zn}(\text{DMF})_6]^{2+}$ to the final $[\text{Zn}(\text{Im})_4]^{-2}$ species studied in the main text. The potential energy computed via *ab initio* calculations and that computed via our force field are in very good agreement. Next, we include two solvent loss reactions $[\text{Zn}(\text{DMF})_6]^{2+} \rightleftharpoons [\text{Zn}(\text{DMF})_5]^{2+} + \text{DMF}$ and $[\text{Zn}(\text{DMF})_5]^{2+} \rightleftharpoons [\text{Zn}(\text{DMF})_4]^{2+} + \text{DMF}$ to probe the relative stability of the different Zn-DMF complexes. Although the magnitudes of ΔE are higher in the DFT calculations, the trend is well reproduced. The differences can be explained by the lack of explicit solvent and thermal effects in the DFT calculations. In addition, we show results for the energy involved in the first ligand addition, described by: $[\text{Zn}(\text{DMF})_4]^{2+} + \text{Im}^- \rightleftharpoons [\text{Zn}(\text{DMF})_4(\text{Im})]^+$ which is also in good agreement with that coming from nb-ZIF-FF. Finally, we compare the stability of the two possible clusters with one ligand moiety: $[\text{Zn}(\text{DMF})_4(\text{Im})]^+ \rightleftharpoons [\text{Zn}(\text{DMF})_3(\text{Im})]^+ + \text{DMF}$. Both the *ab initio* calculations and nb-ZIF-FF predict that the penta-coordinated species is the most stable, although there is a significant difference in energy, which can be explained by thermal and solvent effects as previously mentioned. The energy values are also expected to have a mild dependence on the choice of functional and dispersion corrections.¹⁹ Overall, the stability trends and energies orders of magnitude are correctly captured by our model.

Table 7: Energy differences in kJ/mol for selected Zn-centred cluster interconversion reactions obtained from DFT calculations and via nb-ZIF-FF forcefield.

Reaction	ΔE (DFT)	ΔE (nb-ZIF-FF)
$[\text{Zn}(\text{DMF})_6]^{2+} + 4 \text{Im}^- \rightleftharpoons [\text{Zn}(\text{Im})_4]^{2-} + 6 \text{DMF}$	-153.0	-157.1
$[\text{Zn}(\text{DMF})_6]^{2+} \rightleftharpoons [\text{Zn}(\text{DMF})_5]^{2+} + \text{DMF}$	103.4	36.3
$[\text{Zn}(\text{DMF})_5]^{2+} \rightleftharpoons [\text{Zn}(\text{DMF})_4]^{2+} + \text{DMF}$	136.9	42.0
$[\text{Zn}(\text{DMF})_4]^{2+} + \text{Im}^- \rightleftharpoons [\text{Zn}(\text{DMF})_4(\text{Im})]^+$	-114.3	-126.3
$[\text{Zn}(\text{DMF})_4(\text{Im})]^+ \rightleftharpoons [\text{Zn}(\text{DMF})_3(\text{Im})]^+ + \text{DMF}$	+7.6	+43.0

References

- (1) Raiteri, P.; Laio, A.; Gervasio, F. L.; Micheletti, C.; Parrinello, M. Efficient Reconstruction of Complex Free Energy Landscapes by Multiple Walkers Metadynamics. *The Journal of Physical Chemistry B* **2005**, *110*, 3533–3539.
- (2) Tiwary, P.; Parrinello, M. A Time-Independent Free Energy Estimator for Metadynamics. *The Journal of Physical Chemistry B* **2014**, *119*, 736–742.
- (3) Bussi, G.; Tribello, G. A. *Biomolecular Simulations*; Springer New York, 2019; p 529–578.
- (4) Bennett, T. D.; Simoncic, P.; Moggach, S. A.; Gozzo, F.; Macchi, P.; Keen, D. A.; Tan, J.-C.; Cheetham, A. K. Reversible pressure-induced amorphization of a zeolitic imidazolate framework (ZIF-4). *Chemical Communications* **2011**, *47*, 7983.
- (5) Chalaris, M.; Samios, J. Systematic molecular dynamics studies of liquid N, N-dimethylformamide using optimized rigid force fields: Investigation of the thermodynamic, structural, transport and dynamic properties. *The Journal of Chemical Physics* **2000**, *112*, 8581–8594.
- (6) Ishiguro, S.-i.; Miyauchi, M.; Ozutumi, K. Thermodynamics of formation of binary and ternary complexes of zinc(II) with halide and thiocyanate ions and 2,2'-bipyridine in dimethylformamide. *J. Chem. Soc., Dalton Trans.* **1990**, 2035–2041.

- (7) Park, K. S.; Ni, Z.; Côté, A. P.; Choi, J. Y.; Huang, R.; Uribe-Romo, F. J.; Chae, H. K.; O’Keeffe, M.; Yaghi, O. M. Exceptional chemical and thermal stability of zeolitic imidazolate frameworks. *Proceedings of the National Academy of Sciences* **2006**, *103*, 10186–10191.
- (8) Lewis, D. W.; Ruiz-Salvador, A. R.; Gómez, A.; Rodriguez-Albelo, L. M.; Coudert, F.-X.; Slater, B.; Cheetham, A. K.; Mellot-Draznieks, C. Zeolitic imidazole frameworks: structural and energetics trends compared with their zeolite analogues. *CrystEngComm* **2009**, *11*, 2272.
- (9) Balestra, S. R. G.; Semino, R. Computer simulation of the early stages of self-assembly and thermal decomposition of ZIF-8. *The Journal of Chemical Physics* **2022**, *157*, 184502.
- (10) Castel, N.; Coudert, F.-X. Computation of Finite Temperature Mechanical Properties of Zeolitic Imidazolate Framework Glasses by Molecular Dynamics. *Chemistry of Materials* **2023**, *35*, 4038–4047.
- (11) Gaillac, R.; Pullumbi, P.; Beyer, K. A.; Chapman, K. W.; Keen, D. A.; Bennett, T. D.; Coudert, F.-X. Liquid metal–organic frameworks. *Nature Materials* **2017**, *16*, 1149–1154.
- (12) Giannozzi, P. et al. QUANTUM ESPRESSO: a modular and open-source software project for quantum simulations of materials. *Journal of Physics: Condensed Matter* **2009**, *21*, 395502.
- (13) Prandini, G.; Marrazzo, A.; Castelli, I. E.; Mounet, N.; Marzari, N. Precision and efficiency in solid-state pseudopotential calculations. *npj Computational Materials* **2018**, *4*, 72, <http://materialscloud.org/sss><http://materialscloud.org/ssp>.
- (14) Perdew, J. P.; Burke, K.; Wang, Y. Generalized gradient approximation for the

- exchange-correlation hole of a many-electron system. *Physical Review B* **1996**, *54*, 16533–16539.
- (15) Grimme, S.; Antony, J.; Ehrlich, S.; Krieg, H. A consistent and accurate ab initio parametrization of density functional dispersion correction (DFT-D) for the 94 elements H-Pu. *The Journal of Chemical Physics* **2010**, *132*.
- (16) Andreussi, O.; Dabo, I.; Marzari, N. Revised self-consistent continuum solvation in electronic-structure calculations. *The Journal of Chemical Physics* **2012**, *136*.
- (17) Kandil, M. E.; Marsh, K. N.; Goodwin, A. R. H. Determination of the Relative Permittivity, ϵ_r , of Methylbenzene at Temperatures between (290 and 406) K and Pressures below 20 MPa with a Radio Frequency Re-Entrant Cavity and Evaluation of a MEMS Capacitor for the Measurement of ϵ_r . *Journal of Chemical and Engineering Data* **2008**, *53*, 1056–1065.
- (18) Martyna, G. J.; Tuckerman, M. E. A reciprocal space based method for treating long range interactions in ab initio and force-field-based calculations in clusters. *The Journal of Chemical Physics* **1999**, *110*, 2810–2821.
- (19) Boussouf, K.; Khairat, T.; Prakash, M.; Komiha, N.; Chambaud, G.; Hochlaf, M. Structure, Spectroscopy, and Bonding within the $Zn_q^+ - Imidazole_n$ ($q = 0, 1, 2$; $n = 1-4$) Clusters and Implications for Zeolitic Imidazolate Frameworks and Zn-Enzymes. *The Journal of Physical Chemistry A* **2015**, *119*, 11928–11940.